Fructose-1,6-bisphosphate Acts Both as an Inducer and as a Structural Cofactor of the Central Glycolytic Genes Repressor (CggR)†

Silvia Zorrilla,‡,⊥ Denis Chaix,‡ Alvaro Ortega,‡ Carlos Alfonso,§ Thierry Doan,|| Emmanuel Margeat,‡ Germán Rivas,§ Stephan Aymerich,|| Nathalie Declerck,‡,|| and Catherine A. Royer*,‡

INSERM (U554), Montpellier, France, and Centre de Biochimie Structurale, CNRS (UMR5048), Université Montpellier 1, 29, rue de Navacelles, F-34090 Montpellier, France, Microbiologie et Génétique Moléculaire, INRA (UMR1238) and CNRS (UMR2585), Institut National Agronomique Paris-Grignon, F-78850 Thiverval-Grignon, France, and Centro de Investigaciones Biológicas, CSIC, Ramiro de Maeztu 9, E-28040 Madrid, Spain

Received September 4, 2007; Revised Manuscript Received October 11, 2007

ABSTRACT: CggR is the transcriptional repressor of the *gapA* operon encoding central glycolytic enzymes in *Bacillus subtilis*. Recently, a detailed mechanistic characterization of *gapA* induction revealed that the binding of fructose-1,6-bisphosphate (FBP) to a low affinity site on CggR (K_d > 100 μM) is responsible for repressor release from the DNA. In addition, this prior work demonstrated that FBP binds to a second high affinity site on the repressor, causing a conformational change in the CggR/DNA complexes, but with no consequence on CggR affinity for its operator DNA. In the present study we have thoroughly analyzed the structural and thermodynamic consequences of FBP binding to CggR. Results of fluorescence anisotropy titrations, calorimetry and limited proteolysis confirm the existence in CggR of a high affinity site for FBP, with a K_d of around 6 μM. Using analytical size-exclusion chromatography, ultracentrifugation as well as fluorescence correlation spectroscopy (FCS) and pressure perturbation, we show that FBP binding at this site reduces the size of the CggR oligomers and induces conformational changes that stabilize the dimer against denaturation. Hence, FBP has a dual role on CggR structure and regulatory function. In addition to acting as an inducer of transcription at the low affinity site, FBP bound to the high affinity site acts as a structural cofactor for the repressor, with profound effects on its quaternary structure as well as on its conformational dynamics and stability. This high affinity FBP site apparently evolved from the sugar substrate binding site of homologous enzymes.

In all bacterial cells, the utilization of carbohydrates to provide energy and carbon backbones involves metabolic pathways which are highly regulated at multiple levels. In *Bacillus subtilis*, the enzymes that catalyze the interconversion of triose phosphates in the central part of glycolysis are encoded by the hexacistronic *gapA* operon. Among these enzymes, the NAD-dependent glyceraldehyde-3-phosphate dehydrogenase (GapA) is the most strongly regulated. While the other central glycolytic enzymes are synthesized and active during both glycolysis and neoglucogenesis, GapA is operative only during glycolysis. Similar to plants and cyanobacteria, *B. subtilis* and other Gram-positive bacterial species produce a NADP-dependent dehydrogenase (GapB) to perform the reverse anabolic reaction under neoglucogenic conditions (*1*).

GapA synthesis is controlled at the level of gene expression by two transcriptional regulators: the pleiotropic catabolite control protein A (CcpA), whose indirect regulation mechanism is related to carbohydrate uptake by the cellular phospho-sugar transport system (*2*), and the central glycolytic genes repressor (CggR[1]), which is the product of the first cistron of the *gapA* operon. This repressor was recently identified in the course of a functional analysis of the *B. subtilis* genome (*1*, *3*) . CggR belongs to the SorC family of transcriptional regulators. These repressors contain an N-terminal helix−turn−helix DNA binding motif followed by a regulatory domain involved in inducer binding which is homologous to the NagB enzymes (*37*). Very little information is yet available on the physical parameters underlying the conditional interaction of the SorC family repressors with their operator DNA and effector metabolites. CggR (*4*) and *B. subtilis* DeoR (*5*, *6*) are the only members of this family whose target DNA sequence has been identified, and for which the regulation molecular mechanism has been analyzed from a biophysical point of view.

Fructose-1,6-bisphosphate (FBP) has been identified as the inducer sugar that modulates the interaction of CggR with its target DNA (*4*). FBP is also the most important metabolic

† This work was supported by a Marie Curie intra-European fellowship to S.Z. (MEIF-CT-2004-007320), the Association pour la Recherche sur le Cancer (C.A.R.), INSERM, CNRS and INRA.

* Corresponding author: Centre de Biochimie Structurale, 29, rue de Navacelles, F-34090 Montpellier, France. Tel: 33 (0)4 67 41 79 02. Fax: 33 (0)4 67 41 79 13. E-mail: catherine.royer@cbs.cnrs.fr.

‡ INSERM (U554), Centre de Biochimie Structurale, CNRS (UMR5048), and Université Montpellier 1.

⊥ Present address: Instituto de Química Física "Rocasolano", CSIC, Madrid, 28006 Spain.

§ Centro de Investigaciones Biológicas, CSIC.

|| Microbiologie et Génétique Moléculaire, INRA (UMR1238) and CNRS (UMR2585), Institut National Agronomique Paris-Grignon.

[1] Abbreviations: FBP, fructose-1,6-biphosphate; CggR, entral glycolytic genes repressor; FCS, fluorescence correlation spectroscopy; FCCS, fluorescence cross-correlation spectroscopy.

10.1021/bi701805e CCC: $37.00
Published on Web 12/04/2007

signal for carbon catabolite repression by CcpA (*7*), thus providing a molecular integration point between the CggR and CcpA regulators. FBP is a well-suited modulator molecule, since its concentration in *B. subtilis* shifts considerably with changes in available carbon sources. Indeed, its concentration is ~14 times higher when the bacteria grow in the presence of glucose as opposed to malate (*8*). In addition, FBP is a key metabolite involved in the regulation of the activity of a number of metabolic enzymes such as pyruvate kinase (*9*), glycerol kinase (*10*) and lactate dehydrogenase (*11*).

Recently, we have performed an in-depth analysis of the effects of FBP on the physical parameters governing CggR interactions with its target operator DNA (*12*). Our results demonstrated that CggR binds as a tetramer to the tandem DNA direct repeats constituting the *gapA* operator sequence. We showed that CggR binds to the full-length operator in a highly cooperative manner and that FBP does not change the stoichiometry of the CggR/DNA complexes. However, the cooperativity of binding and, thus, the overall apparent affinity decrease dramatically in the presence of millimolar concentrations of inducer. In addition to this low affinity FBP binding implicated in the induction mechanism, we discovered that the CggR/operator complexes also responded to FBP in the micromolar range. FBP binding at this high affinity site led to a clear modification of the conformational dynamics of the repressor/operator complexes, but had no effect on DNA binding.

In the present study, we sought to examine the effect of FBP on the physical properties of the CggR protein alone in order to better define the biological role of this high affinity binding site. The consequences of FBP binding on the quaternary structure, hydrodynamics, stability, and conformation of CggR were investigated by a combination of analytical methods including chromatography, ultracentrifugation, fluorescence anisotropy, calorimetry, limited proteolysis and pressure perturbation. The results of these analyses showed that FBP interferes with CggR self-association and confirmed the existence of two classes of FBP binding sites on the repressor. The affinity of FBP for the high affinity site was determined by steady-state anisotropy-based titrations and isothermal titration calorimetry. We showed that at this site, FBP binding favors CggR dimers and stabilizes the protein against denaturation. Finally, we used fluorescence correlation spectroscopy (FCS) in order to characterize FBP-driven effects on the CggR molecules in the more physiologically relevant nanomolar range of protein concentration. Together with our previous DNA binding studies, our results demonstrate that FBP acts not only as the inducer sugar that modulates the interaction of CggR with the *gapA* operator but also as a structural cofactor of the repressor protein.

MATERIALS AND METHODS

Protein Expression and Purification. CggR was produced in *Escherichia coli* strain M15pREP4 using pQE30 expression vector (Qiagen), and the His-tagged protein was purified by affinity chromatography followed by size exclusion chromatography as described previously (*4*, *12*). It was shown that the N-terminal His-tag does not alter the CggR repressor function (*4*). Protein concentration was determined by both Bradford assay and UV absorbance at 280 nm, using a theoretical extinction coefficient of 14770 M^{-1} cm^{-1}.

Cross-Linking and Size Exclusion Chromatography. Purified CggR was dialyzed overnight in 50 mM Na-phosphate buffer (pH 8.0), NaCl 150 mM, 1 mM DTT. Protein aliquots at 0.5 mg/mL, supplemented or not with 2 mM FBP, were incubated with glutaraldehyde (grade I 25% aqueous solution, Sigma) at a final concentration of 0.025%. After 5 or 30 min incubation at room temperature, the reaction was stopped by adding Tris (pH 8) at a final concentration of 100 mM and the cross-linked material was analyzed by SDS−PAGE on 10% polyacrylamide gels and Coomassie-blue staining. Size exclusion chromatography experiments were carried out using a Superdex200-HR10/30 gel filtration column (GE Healthcare). 200 μL of a purified CggR sample in 50 mM Tris-HCl, 150 mM NaCl, 2 mM EDTA, 2 mM TCEP, pH 8 containing either no FBP or 2 mM FBP was injected onto the column, and elution was monitored at 280 nm.

Limited Proteolysis Assays. Proteolysis reactions were carried out in 25 mM Tris-HCl buffer, pH 8.0, containing 10 mM $CaCl_2$, using Trypsin (Sigma-Aldrich Co) at 0.15 mg/mL. CggR concentration was 12.4 nM, and the samples also contained increasing concentrations of FBP (1 μM to 5 mM). The enzyme/substrate volume ratio was 1:5, and proteolytic digestion was allowed to proceed at 30 °C for 5 or 30 min. Proteolytic digestion was stopped by addition of concentrated SDS−PAGE sample buffer to a final concentration of 0.01 M Tris-HCl, pH 6.8, 1% SDS, 5% 2-mercaptoethanol (v/v) 50 mM EDTA, 1.36 M glycerol, 0.0025% bromophenol blue. The samples were immediately heated in a boiling bath for 5 min and kept on ice until being loaded on a 15% SDS−PAGE. We have verified on an unrelated protein (PlcR) that FBP does not affect trypsin activity (unpublished results).

Analytical Ultracentrifugation Experiments. Sedimentation velocity experiments were carried out using an Optima XL-A analytical ultracentrifuge (Beckman-Coulter, Palo Alto, CA) equipped with a UV−visible absorbance detection system. A Ti60 eight-hole rotor and standard (12-mm optical path) double sector centerpieces of Epon-charcoal were used. 23 μM CggR samples were centrifuged at 40 krpm at 10 °C. The buffer for the measurements was 50 mM Tris-HCl, 150 mM NaCl, 2 mM EDTA, 2 mM TCEP, pH 8.

CggR sedimentation coefficient distributions were determined by direct linear least-squares boundary fitting of the sedimentation velocity profiles using the software SEDFIT (*13*). For the correction of *S* values to standard conditions (20 °C and water), the software SEDNTERP (retrieved from the RASMB server (*14*)) was used. The same software was used to estimate the partial specific volume of CggR from its amino acid sequence and the buffer viscosity and density at different temperatures.

Hydrodynamic Modeling. The low-resolution hydrodynamic model of CggR was built employing the simulation program HYDROPRO (*15*) for calculation of hydrodynamic properties from the atomic structures of each of the two domains of the repressor. Then, each domain was modeled as a revolution ellipsoid that best reproduced the hydrodynamic properties calculated by HYDROPRO, using and minimizing an optimization function that allows us to compare the properties calculated for different sizes and

ratios of revolution ellipsoids with the ones calculated from the atomic coordinates. The model was further validated by calculation of the eigenvalues of the gyration tensor for each domain from the atomic structures using the program ORIEL (*16*), which yields the length of the semiaxis of the ellipsoid that best reproduces this gyration tensor. The results for these values were in perfect agreement with those calculated from the hydrodynamic properties. The program HYDROSUB (*17*), which utilizes the bead-shell model extrapolation approximation to calculate the properties of structures made of simple symmetrical subunits, was used to calculate the hydrodynamic properties of the low-resolution model built.

Isothermal Titration Calorimetry Experiments. ITC experiments were performed using the VP ITC system (MICROCAL). 1.3 mL of a 12 μM protein solution was titrated with 300 μL of a 200 μM solution of the inducer metabolite FBP. 30 injections of 5 μL were performed. The buffer for the experiments was 20 mM Hepes, 150 mM NaCl, 2 mM TCEP, pH8. The analysis of the binding curves was performed using the software Microcal ORIGIN. The experiment was carried out three times with the same result.

Fluorescent Labeling of CggR. CggR was covalently labeled with tetramethylrhodamine succinimidyl ester (Molecular Probes, Invitrogen), alexa Fluor 488 (Molecular Probes, Invitrogen) and atto 647N (atto-Tec, GmbH) carboxylic acid succinimidyl ester dyes in the amine groups, directly after eluting from the Ni^{2+}-NTA agarose column during the purification protocol. A 10-fold molar excess of the dye was added drop by drop to a solution of CggR, and the reaction was allowed to proceed at room temperature for 2 h with continuous agitation. The reaction buffer was 0.1 M sodium phosphate, 50 mM NaCl, 2 mM TCEP, pH 8 for labeling with tetramethylrhodamine succinimidyl ester and 0.1 M sodium bicarbonate, 150 mM NaCl, 2 mM TCEP, pH 8.3 for the other two dyes. The reaction was stopped by adding 10% Tris-HCl 1M. The mixture was loaded onto a PD 10 desalting column (GE Healthcare) and purified trough a Superdex 200XK 16/70 column (GE Healthcare) equilibrated in 10 mM Tris-HCl, 150 mM NaCl, 2 mM DTT and 2 mM EDTA pH 8 buffer. The ratio of labeling was estimated using the extinction coefficient of the dyes provided by the suppliers, 65000, 71000, 150000 M^{-1} cm^{-1} for tetramethylrhodamine at 555 nm, alexa 488 at 495 nm and atto 647N at 644 nm, respectively and that of CggR, 14700 M^{-1} cm^{-1} at 280 nm. The protein concentration was also measured by Bradford assay. In this way the degree of labeling was found to be 30%, 10% and 65% for tetramethylrhodamine, alexa 488 and atto 647N labeling, respectively.

Fluorescence Anisotropy Binding Assays. Steady-state fluorescence anisotropy binding titrations were carried out using a Beacon 2000 Fluorescence Polarization System (Panvera Corp., Madison WI) equipped with automatic temperature control. TMR labeled CggR (TMR-CggR) titrations were performed by adding increasing concentrations of nonlabeled protein or FBP inducer to independent tubes containing a fixed amount of TMR-CggR. Anisotropy values plotted represent the average of 5−7 values measured by the instrument after equilibration. Each curve is the average of 3 independent experiments. The buffer for the measurements was 50 mM Tris-HCl, 150 mM NaCl, 1% glycerol, 0.05 mg/mL BSA, 2 mM EDTA, 2 mM DTT, pH 8 and the temperature was 21 °C. The concentration of TMR-CggR was 27 nM in the titrations with nonlabeled CggR and 37 nM in the titrations with FBP.

Analysis of the experimental binding curves was conducted using Bioeqs software (*18*−*20*). This software allows the determination of the free energies of formation of the postulated complexes from the individual elements by using a numerical solver. The error in the determined free energies was estimated using rigorous confidence limit testing at the 67% confidence level, in which the uncertainties arising from parameter correlations were taken into account.

Time-Resolved Fluorescence Spectroscopy Experiments. Time-resolved fluorescence measurements were conducted using an ISS KOALA sample chamber and ISS analog frequency domain electronics (ISS, Inc. Champaign IL). The sample was excited at 450 nm by frequency doubling of the pulse picked emission at 900 nm of a Spectra Physics Tsunami tunable Ti:sapphire infrared mode-locked picosecond laser pumped by a 10 W Millenia diode laser. Emission was observed via a monochromator at 520 nm. Fluorescein in a buffered solution pH 9.0 was used as the reference lifetime compound. Phase and modulation data were collected until errors were less than 0.3 and 0.005 degrees of phase and modulation units, respectively. Excitation was vertically polarized and emission was set at magic angle for lifetime measurements. In the samples, alexa 488 labeled CggR concentration was 3 μM. The buffer and the temperature (21 °C) were the same as for the anisotropy binding titrations.

For data analysis the Globals software (Laboratory of Fluorescence Dynamics, Urbana, IL) was used. This program is based on a nonlinear least-squares procedure to minimize the squared deviations between the observed and expected phase and modulation values for multiple experimental data sets. Correlated error analysis (i.e., one parameter is varied near the minimum while the other parameters are all free) was performed on the rotational correlation times, and the rigorous 67% confidence limits are reported for each parameter. For lifetime analysis, a model involving a double exponential fluorescence intensity decay, $I(t)$, was found to adequately describe the experimental data:

$$I(t) = \alpha_1 \exp(-t/\tau_1) + \alpha_2 \exp(-t/\tau_2) \qquad (1)$$

where τ_i is the fluorescence lifetime and α_i, the pre-exponential factor ($\alpha_1 + \alpha_2 = 1$). When analyzing the anisotropy decays, $r(t)$, a double-exponential model was found to best fit the experimentally recovered decays:

$$r(t) = r(0)[\beta_1 \exp(-t/\phi_1) + \beta_2 \exp(-t/\phi_2)] \qquad (2)$$

where $r(0)$ is the time-zero anisotropy, ϕ_i are the rotational correlation times and β_i the fractional amplitude of each rotational correlation time ($\beta_1 + \beta_2 = 1$).

Fluorescence Correlation and Cross-Correlation Spectroscopy. FCS measurements were carried out on a FCS setup based on a dual channel ISS Alba fluorescence correlation detector with avalanche photodiodes connected to a Zeiss Axiovert 200 microscope. Excitation of the sample was achieved by means of a two photon Spectra Physics Mai Tai HP femtosecond IR tunable laser set at 780 nm, focused into the sample by a Zeiss Apochromat 63X oil immersion

objective (numerical aperture 1.4). The excitation power was set at 10 mW at the scope entrance. Care was taken to avoid both photobleaching and excitation saturation effects (*21*) by testing the excitation power dependence of the Go and autocorrelation profiles, and a threshold excitation power was determined to be that at which the profiles became excitation power independent. An E700 SP 2P dichroic filter (Chroma Technology Corporation) was used to eliminate the IR exciting light in the emission. In the FCS measurements carried out using TMR-CggR, a 565 nm dichroic mirror was used to split the detected light onto two channels and an additional 610 ± 75 nm band-pass emission filter was placed before channel 1. When performing the cross-correlation measurements using alexa 488 and atto 647N labeled CggR, the same dichroic mirror was used but a 675 ± 50 nm and a 525 ± 50 nm band-pass filters were set before channel 1 and 2 respectively. For the measurements 8-well Lab-Tek chambers, were used. The chamber wells were coated with a 10 mg/mL BSA solution, and the samples were loaded after extensive rinsing with buffer. The sampling frequency was 500 kHz and the time of measurement 40 s. Calibration of the system was performed with a fluorescein solution of known concentration measured under the same illumination conditions as the samples. In our experiments, autocorrelation curves were acquired at CggR concentrations in between (60 nM and 1.2 μM) in the presence and in the absence of different FBP concentrations (10 μM, 100 μM, 2 mM and 10 mM). Protein concentrations above 300 nM were achieved by adding nonlabeled CggR to 300 nM TMR-CggR. Cross-correlation measurements were carried out using samples containing a mixture of alexa 488 and atto 647N labeled CggR, at 700 nM total repressor concentration, in the absence and in the presence of 10 mM FBP. For each sample, autocorrelation functions were acquired 5 times and the data in the graphs and tables represent the average of at least 3 independent experiments. The buffer for the measurements was 50 mM Tris-HCl, 150 mM NaCl, 1% glycerol, 0.05 mg/mL BSA, 2 mM EDTA, 2 mM DTT, pH 8.

In a two-photon fluorescence correlation spectroscopy experiment, the fluctuations in the fluorescence intensity detected in a small open volume defined by two-photon excitation probability are measured and time-correlated to generate an autocorrelation function:

$$G(\tau) = \langle \delta F(t) \langle \delta F(t+\tau) \rangle / \langle F(t) \rangle^2 \quad (3)$$

where τ is the lag time. When considering a system of freely diffusing monodisperse and uniformly bright fluorescent molecules, the following expression is derived:

$$G(\tau) = (\gamma/N) \sum_i [f_i (1 + \tau/\tau d_i)^{-1} (1 + {\omega_0}^2 \tau / {z_0}^2 \tau d_i)^{-1/2}] \quad (4)$$

where γ is the geometric factor, which constitutes a measure of the uniformity of the fluorescence intensity observed for molecules at different positions within the detection volume. The parameters ω_0 and z_0 are the width and length, respectively, of the three-dimensional Gaussian excitation volume at which the intensity drops to $1/e^2$. The parameter, τd_i is the translational diffusion time, f_i is the fractional contribution of species i to the autocorrelation function and N, the average number of molecules.

In a two-photon cross-correlation experiment, two spectrally different fluorophores are simultaneously excited and the fluctuations in the intensity emitted by each of them are detected in two individual channels (1 and 2) and time-correlated to generate three separate functions, the autocorrelation function of each of the fluorophores and the cross-correlation function, which accounts for the molecules bearing the two fluorophores. Under ideal conditions with no cross-talk, the cross-correlation function $G_{12}(\tau)$ becomes

$$G_{12}(\tau) = \langle \delta F_1(t) \langle \delta F_2(t+\tau) \rangle / \langle F_1(t) \rangle \langle F_2(t) \rangle \quad (5)$$

If we consider that the species present in the solution are only species 1 and 2 and the complex 12, then eq 4 becomes

$$G_{12}(\tau) = G(0)(1 + \tau/\tau d_{12})^{-1} (1 + {\omega_0}^2 \tau / {z_0}^2 \tau d_{12})^{-1/2} \quad (6)$$

where τd_{12} is the diffusion time of the complex and $G(0)$ is the amplitude.

Data analysis was performed with the ISS Vista software. This program uses a Marquardt−Levenberg minimization algorithm, and the goodness of the fittings can be judged by the recovered χ^2. In the analysis a Gaussian model was selected for describing the laser point spread function and the beam waist, ω_0, and height, z_0, were fixed to that obtained by calibration with the fluorescein solution. The beam waist ω_0 was found to be near diffraction limited, 0.4 μm, and the z_0 was about 1 μm with an excitation at 780 nm. All of the recovered autocorrelation and cross-correlation curves $G(\tau)$ were best fit using a model involving two diffusing components:

$$G(\tau) = \gamma/N[f_1(1 + \tau/\tau d_1)^{-1}(1 + {\omega_0}^2 \tau / {z_0}^2 \tau d_1)^{-1/2}] [f_2(1 + \tau/\tau d_2)^{-1}(1 + {\omega_0}^2 \tau / {z_0}^2 \tau d_2)^{-1/2}] \quad (7)$$

where τd_i and f_i are the translational diffusion time and the fractional contribution to the autocorrelation function of the ***i***th component. N is the average number of fluorescent molecules in the sample volume. In two photon excitation, the translational diffusion time, τd_i, of the fluorescent species is related to the diffusion coefficient, D_i, by the equation

$$D_i = z_0/(8\tau d_i) \quad (8)$$

Since our experiments were carried out using two-photon excitation, our data analysis did not require taking into account triplet states. For each protein concentration, the curves recovered at different FBP concentrations were globally analyzed in terms of a consistent set of parameters by linking the diffusion coefficients across the curves and allowing their relative contribution to vary from one curve to another. The average translational diffusion coefficient $\langle D \rangle$ was calculated as a mean of the two recovered translational diffusion times (D_i) weighted by their fractional contribution to the autocorrelation function (f_i):

$$\langle D \rangle = (D_1 f_1 + D_2 f_2) \quad (9)$$

High-Pressure Perturbation Experiments. High-pressure fluorescence measurements were conducted using a stainless steel high-pressure vessel similar to that described previously (*22*). The sample was excited by a 300 W xenon arc lamp through a fiber-optic cable coupled to the ISS Koala

spectrofluorimeter (ISS, Inc., Urbana, IL). The excitation wavelength was 295 nm and the slits were 1 and 2 nm in excitation and emission, respectively. The pressure transducing liquid was water, and the 0.6 mL cell was sealed with Duraseal and an O-ring. The experiments were carried out at 21 °C, and the protein concentration was 25 μM. The buffer was 50 mM Tris-HCl, 150 mM NaCl, 2 mM DTT, pH 8. The center of the spectral mass (or average emission wavelength), $\langle\lambda\rangle$, was calculated, using the ISS Vinci software, as

$$\langle\lambda\rangle = \sum F_i\lambda_i / \sum F_i \qquad i = 317, 318, ..., 420 \text{ nm} \qquad (10)$$

where F_i is the fluorescence intensity at an emission wavelength of λ_i nm.

RESULTS

FBP Reduces the Size of CggR Oligomers. The effect of FBP on the oligomeric state of CggR was first investigated by analytical size exclusion chromatography (Figure 1A). While purifying the protein, we noticed that the purified repressor had a strong tendency to precipitate in concentrated solution but remained soluble below 2.5 mg/mL (63 μM). When a 200 μL purified protein sample at 13 μM was injected on a Superdex200-HR10/30 gel filtration column, the protein was eluted as a major peak in the exclusion volume, indicating that CggR is essentially present as oligomers of molecular weight exceeding the resolution of the column. Adding FBP at 2 mM in the protein sample, and at 0.5 mM in the column buffer, considerably reduced the size of these oligomeric species and spread out the protein elution profile. A significant amount of low molecular weight material could be detected in the presence of FBP, in particular in peaks centered around 14 and 12.5 mL, corresponding to an apparent molecular weight of about 80 and 140 kDa, respectively. The theoretical molecular weight of the His-tagged protomer being 38.7 kDa, it can be concluded that CggR polypeptide chains remain associated at least as dimers even in the presence of FBP.

Cross-linking experiments followed by SDS−PAGE analysis of the covalently bound CggR protomers were conducted with the purified protein at 0.5 mg/mL in phosphate buffer (Figure 1B). After 30 min reaction with 0.025% glutaraldehyde, only a diffuse band corresponding to high molecular weight cross-linked materials remained visible, confirming the presence of high order oligomers of CggR. When 2 mM FBP was added to the reaction medium, the amount of cross-linked protein was noticeably reduced, while the band at 37 kDa corresponding to the CggR protomer persisted over the entire incubation time. In addition, discrete bands of about 80 and 110 kDa were detected that could correspond to cross-linked dimers or trimers.

The oligomerization state of CggR was further investigated by analytical ultracentrifugation (Figure 2A). Sedimentation velocity (SV) experiments were conducted on protein samples containing 23 μM CggR (0.89 mg/mL) in the absence and in the presence of 2 mM FBP. The SV profiles were analyzed in terms of a distribution of sedimentation coefficients, which allowed for evaluation of solute homogeneity. CggR solutions were found to be highly heterogeneous and to contain a high proportion of rapidly sedimenting complexes corresponding to high molecular weight molecular species. Note that in such velocity experiment, very high molecular weight materials are pelletted in the first minutes of the run and are therefore not visible. It is also noteworthy that the sedimentation coefficient distribution depended on protein concentration and experimental conditions. Addition of 2 mM FBP reproducibly provoked a global shift of the profiles recovered for the repressor protein toward lower sedimentation coefficient values and increased the relative amount of low molecular weight species. All together, these experiments demonstrate that the CggR repressor forms high order oligomers whose size is reduced in the presence of FBP.

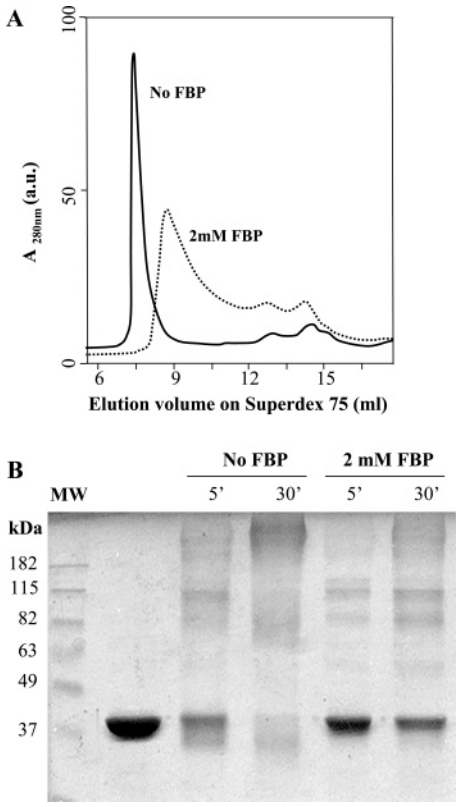

FIGURE 1: Effect of the modulator ligand FBP on CggR oligomerization. (A) Size exclusion chromatography of purified CggR in the absence (solid line) or in the presence (dotted line) of FBP. Elution profile on Superdex 200 HR10/30 prepacked column (GE Healthcare) of 200 μL aliquot of 0.5 mg/mL purified His-tagged CggR solutions, monitored by absorbance at 280 nm. For the experiment in the presence of the inducer sugar, FBP was added at a final concentration of 2 mM to the protein sample and 0.5 mM to the column equilibration buffer (10 mM Tris-HCl (pH 8), 150 mM NaCl, 2 mM DTT, 2 mM EDTA). (B) Cross-linking by glutaraldehyde in the absence or in the presence of 2 mM FBP. SDS−PAGE analysis of the cross-linked CggR protomers after 5 and 30 min reaction with 0.025% glutaraldehyde at room temperature. After overnight dialysis in 50 mM Na-phosphate buffer (pH 8), NaCl 150 mM, 1 mM DTT, 100 μL aliquots of purified His-tagged CggR at 0.5 mg/mL were incubated. The His-tagged protein was dialyzed overnight in and incubated in phosphate buffer absence and in 2 mM FBP solution.

CggR Forms Asymmetrical Dimers. The putative molecular weights of the CggR oligomers corresponding to the peaks observed in the sedimentation velocity experiments were first calculated assuming spherical complexes. The fastest sedimenting species observed in the absence of FBP, around 23.4 S, corresponds to a molecular weight exceeding 700 kDa, which decreases to around 500 kDa in the presence of FBP. FBP binding leads to smaller *S* values for all of the

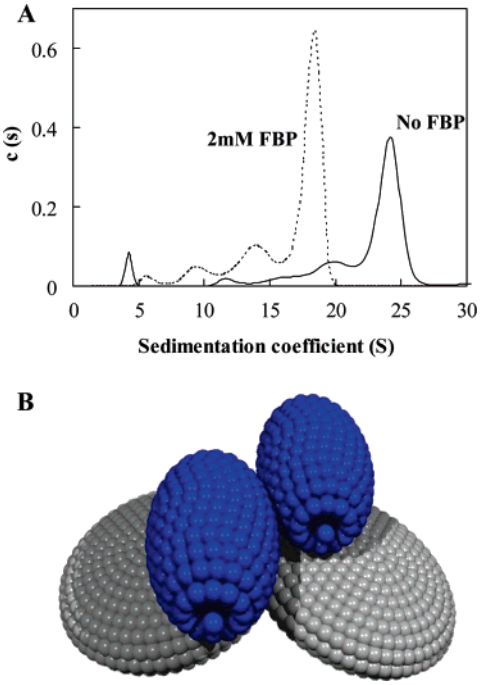

FIGURE 2: Sedimentation coefficient distributions and low-resolution hydrodynamic model of CggR. (A) Sedimentation coefficient distributions of CggR in the absence (solid line) and in the presence (dotted line) of 2 mM FBP corrected to standard conditions (20 °C). $\lambda = 280$ nm. CggR concentration was 23 μM. (B) Bead shell model of the low-resolution structure of the CggR dimer. This model predicts correctly the hydrodynamic properties obtained in laboratory for the wild type CggR protein.

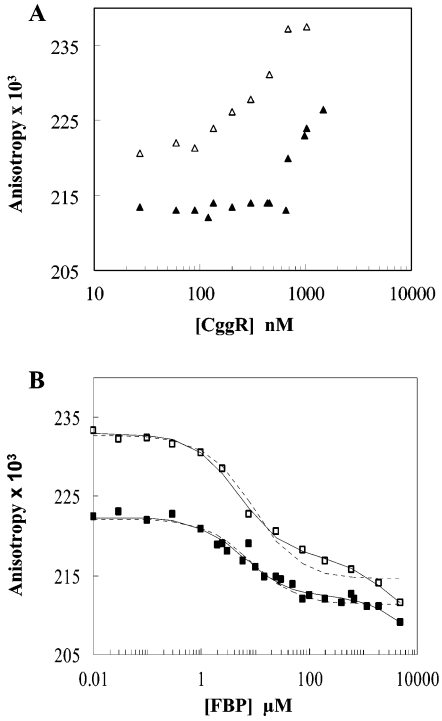

FIGURE 3: Concentration dependent CggR oligomerization and FBP binding monitored by steady-state fluorescence anisotropy. (A) TMR-CggR titrations with additional unlabeled CggR in the absence (open triangles) and in the presence (closed triangles) of 2 mM FBP. The concentration of labeled CggR was 27 nM. (B) FBP binding by CggR monitored by steady-state fluorescence anisotropy. CggR-TMR concentration was 37 nM. In the curve represented by open squares, 463 nM additional unlabeled CggR was added for a 500 nM total CggR concentration. Solid lines correspond to a fit using a model in which two different affinity binding sites were considered for FBP while the dashed ones correspond to models assuming a single binding site. The errors in the data are within the symbols.

species, except the slowest sedimenting one. In the presence of FBP, the sedimentation coefficient of the peak at 5.6 S is at the upper limit of what one might expect for a spherical dimer of 77 kDa. However, this peak could also represent trimers or, more likely, a combination of dimers and tetramers. In the absence of inducer the slowest sedimenting species exhibits a sedimentation coefficient of 4.3 S, smaller than expected for a spherical dimer (5.2 S), but too high for a monomer (3.3 S). Since we have no information about the shape of these complexes, we have plotted the *S*-value distributions, rather than calculating an apparent molecular weight.

In order to ascertain whether an asymmetrical dimer could account for this slowly sedimenting species in the absence of inducer, we constructed a low-resolution model of full-length CggR in order to estimate its putative hydrodynamic properties. The crystal structure of the full-length protein was recently solved in the context of the Midwest Structural Genomics Program, and the coordinates for this structure have recently been deposited in the Protein Data Bank (pdb code 2OKG). However, only the regulatory domain (residues 88−338) is visible in this structure, the N-terminal winged helix−turn−helix (wHTH) DNA binding domain (DBD) being too mobile or heterogeneous to be resolved. Interestingly, two polypeptide chains form the asymmetric unit of the 1OKG crystal structure. Based on this structure, we first constructed a low resolution double prolate ellipse model of the dimeric regulatory domain. Using sequence comparison and molecular threading, we predicted that the N-terminal DBD of CggR most resembles the MarR/AsrR-type winged-helix motifs (*37*). A prolate ellipse model of the CggR DBD was thus constructed based on the coordinates of MarR, and the two monomers were placed in multiple orientations with respect to those of the regulatory domain. One of the resulting hydrodynamic models of full-length CggR is shown in Figure 2B. The hydrodynamic properties of these low-resolution models were calculated using the program HYDROSUB (*17*): Regardless of the relative orientation of the DBDs, all models yielded nearly identical translational diffusion coefficients (53−54 $\mu m^2/s$) and sedimentation coefficients (4.3−4.4 S) The rotational correlation time is significantly more sensitive to shape and was found to be between 65 and 90 ns. The sedimentation coefficient of 4.3−4.4 S estimated for dimeric CggR is in very good agreement with the lowest sedimentation coefficient value observed in the absence of FBP. Thus, our results support the conclusion that the smallest observed species for CggR in the sedimentation experiments can be modeled as an asymmetrical dimer, and given the relative insensitivity of the translational diffusion to conformational flexibility, this species is unlikely to correspond to a flexible monomeric species (*23*).

CggR Has Two Classes of FBP Binding Sites. Our previous DNA binding studies have shown that the induction of the *gapA* operon depends on saturation of a millimolar affinity FBP site on CggR (*12*). These studies also revealed the presence of a micromolar affinity FBP binding site on CggR, the saturation of which modifies the nanosecond dynamics of the CggR/operator DNA complexes, but not the

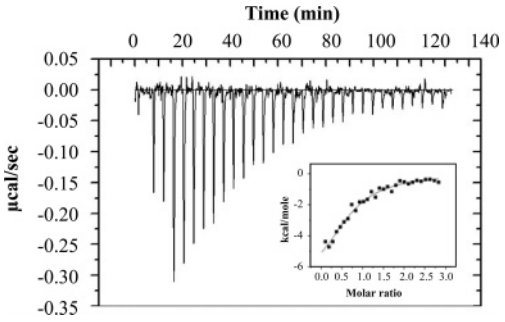

FIGURE 4: Isothermal titration calorimetry profile of FBP binding by CggR. The fit shown corresponds to a model in which only one binding site was postulated. In the experiment, the CggR concentration was 12 μM and the stock FBP concentration, 200 μM.

CggR/operator binding thermodynamics (*12*). Here we sought to directly probe the interaction of CggR with its sugar ligand by fluorescence-based anisotropy titration. The protein concentration dependence of the fluorescence anisotropy of tetramethylrhodamine (TMR) labeled CggR was determined in the absence and in the presence of 2 mM FBP (Figure 3A). In the absence of FBP, a significant anisotropy increase was observed upon increasing the CggR concentration above 100 nM, reflecting the formation of higher order oligomers. Addition of 2 mM FBP noticeably shifted this profile to higher protein concentration, indicating (as in the sedimentation velocity experiments) that FBP disfavors the formation of CggR oligomers.

FBP titrations were carried out in solutions of 37 nM TMR-labeled CggR alone and in the presence of 463 nM unlabeled CggR (Figure 3B). In both cases, a significant decrease in the anisotropy of the TMR label was observed between 1 and 100 μM of FBP, indicating that a binding event takes place in the micromolar range of concentration. The apparent dissociation constants determined for the binding of FBP to this high affinity site were 6.3 μM ($\Delta G^\circ = -7.0 \pm 0.4$ kcal/mol) and 4.4 μM ($\Delta G^\circ = -7.2 \pm 0.2$ kcal/mol) for 37 nM and 500 nM CggR, respectively. These free energies are only apparent since, as stated above, at the higher CggR concentration, the protein begins to populate higher order species (as shown by FCS, see below). Moreover, it is informative to consider that even though only 30% of the protein is labeled with the fluorescent dye, the coexistence of ~20 nM or even ~490 nM unlabeled protein does not have any incidence on the apparent K_d. This is because the experiments are carried out under equilibrium conditions and the total ligand concentration is sufficient to saturate both the labeled and unlabeled species. We have carried out simulations of binding using higher and higher concentrations of competing unlabeled CggR. Indeed, significant deviations from the binding curve only occur at concentrations of unlabeled CggR above 5 μM. Some evidence for the second, millimolar affinity site is observed at high FBP and protein concentrations, but the value of its free energy of binding is not well resolved from the present data. In our earlier work this second (low affinity) site was amply demonstrated to be responsible for the decrease in CggR-DNA interactions.

FBP binding by the repressor protein in the micromolar range was further analyzed by isothermal titration calorimetry (ITC) (Figure 4). The ITC data were best fit to a single species model with an apparent dissociation constant of 7 μM ($K = 1.4 \times 10^5 \pm 2.9 \times 10^4$), in good agreement with the steady-state fluorescence anisotropy determinations. Thus, our anisotropy binding titrations, together with the ITC experiments, confirm the presence of a high affinity FBP binding site with an apparent K_d in between 4 and 7 μM.

Table 1: Time-Resolved Fluorescence Anisotropy Parameters of CggR at Variable FBP Concentration[a]

[FBP] (mM)	0	0.01	0.1	2
ϕ_{fast} (ns)	0.5 ± 0.1	0.5 ± 0.1	0.55 ± 0.07	0.44 ± 0.07
ϕ_{slow} (ns)	27 (−2;+23)	27 (−4; +19)	27 (−4;+8)	21 (−3;+6)

[a] CggR concentration was 3 μM. The $r(0)$ recovered from the fittings was 0.38 ± 0.01, and the amplitude of the fast rotational correlation time (ϕ_{fast}) was 0.44 ± 0.02. The errors were determined from rigorous confidence limit testing at the 67% confidence level.

FBP Modulates the Conformational Dynamics of CggR. The data in Figure 3A indicate that CggR exhibits a protein concentration dependent oligomerization that is disfavored by FBP, however the observed changes in anisotropy may not directly reflect changes in the size of the complex since the correlation time estimated for the dimer is at the limit of the resolution of the dye (~10-fold the fluorescence lifetime). Likewise, the decrease in anisotropy observed upon addition of FBP clearly demonstrates that FBP binds to the protein in the micromolar range, however, the changes in anisotropy could arise, at least in part, from changes in conformational dynamics, rather than directly reflecting the change in oligomerization state. To investigate the possibility of FBP-induced changes in conformational dynamics, we carried out time-resolved fluorescence experiments as a function of FBP concentration (0 to 2 mM). Due to the technical constraints of our laser system, we used, in this case, CggR labeled with alexa 488 (3 μM). The experimental intensity decays were best fit to a double exponential model, with recovered lifetimes of 3.8 ± 0.2 and 0.6 ± 0.2 ns. The decays were dominated by the longest lifetime, whose fractional contribution was 94%. The anisotropy decays were best described by a biexponential function as well, with a short rotational correlation time of 0.5 ± 0.1 ns, whose fractional contribution to the decay was 0.44 ± 0.02. The time-zero anisotropy was found to be 0.38 ± 0.1 in all cases. The short rotational correlation time observed corresponds to the local motion of the alexa 488 dye covalently bound to the repressor. The long rotational correlation time, with values between 20 and 30 ns (Table 1), was generally not well resolved and decreased progressively upon addition of FBP. Under the labeling conditions used (pH 8.3), the N-terminus is considerably more reactive than the lysine residues, and hence it is highly unlikely that the labeling itself is heterogeneous, particularly at the low labeling ratio (10%) obtained here. However, regardless of whether the two lifetime and/or rotational correlation time components arise from the heterogeneous motions of the dye at one site, or the homogeneous motions (one fast and one slow) of the dye at two distinct sites, the point is that we observe this long correlation time, in addition to the fast local rotation of the dye. Interestingly, this long rotational correlation time is shorter than the global tumbling predicted by our model for dimeric CggR (between 65 and 90 ns), and at 3 μM, CggR forms already oligmers of higher order than dimer. We conclude, therefore, that CggR oligomers display local motions on intermediate time scales, and that binding of FBP modulates

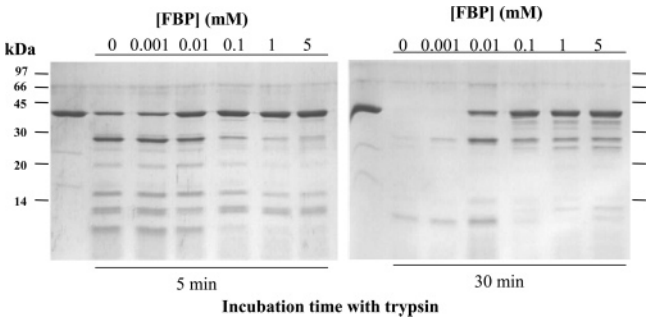

FIGURE 5: Effect of FBP binding on the trypsin sensitivity of CggR. SDS−PAGE analysis of the trypsin digestion of CggR in the presence of increasing concentrations of the inducer at 5 and at 30 min. CggR concentration was 12.4 μM.

these conformational dynamics, in addition to decreasing the oligomeric state of the protein.

FBP High Affinity Binding Protects CggR against Trypsin Degradation. We previously performed limited proteolysis studies with purified CggR and observed that addition of 2 mM FBP drastically reduced the trypsinolysis kinetics (*37*). From this observation, we concluded that FBP binding changed the conformation of the CggR molecules which became more stable, as often observed for ligand-bound proteins. Here we investigated the protective effect of FBP over a range of sugar concentrations from 1 μM to 5 mM. In the gels presented in Figure 5, protection of the repressor against proteolytic cleavage upon addition of inducer is clearly observed. After 30 min incubation with trypsin, CggR in 0.5 mg/mL protein solution containing no or 1 μM FBP was totally degraded. In contrast, the band corresponding to the intact protein persisted in the presence of FBP at 10 μM and above. This further confirms that FBP interacts with CggR in the micromolar range, and indicates that binding at this high affinity site stabilizes the repressor structure. Interestingly, two distinct degradation patterns were observed depending on FBP concentration. At 10 μM and below, a proteolytic fragment of about 27 kDa accumulated in the protein solution before further hydrolysis, whereas at high FBP concentration, multiple degradation bands were visible. We observed similar trypsinolysis patterns in our previous study and established by N-terminal sequencing of the 27 kDa fragment that the primary cleavage of CggR occurs at residues Arg250 and Arg251 in the absence of FBP (*37*). From the present study it can be concluded that the protein region containing these residues undergoes stabilizing conformational changes upon FBP binding at the high affinity site. At higher inducer concentrations it appears that additional cleavage sites become available, indicating an FBP induced change in tertiary or quaternary structure over this range.

FBP Stabilizes CggR Dimers against Pressure Perturbation. Several studies have demonstrated that the application of pressure leads to the dissociation of oligomeric proteins into their respective subunits (*24*). Moreover, since the protein−solvent system occupies a smaller volume when the protein is in the unfolded state, the application of pressure can lead to the unfolding of native proteins (*25*−*27*). Here, the pressure perturbation approach has been used to investigate the effect of FBP binding on the self-association/stability of CggR. In our experiments, the intrinsic fluorescence of the single tryptophan residue of CggR has been

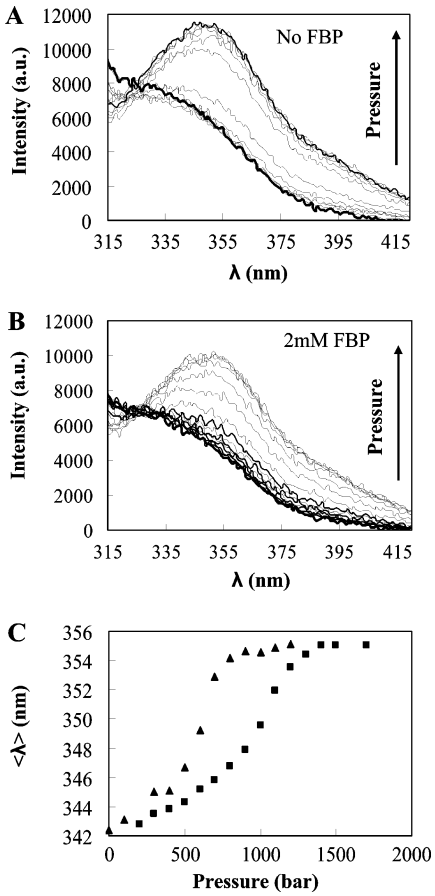

FIGURE 6: Pressure-dependence of CggR intrinsic fluorescence in the presence and in the absence of 2 mM FBP. Emission spectra of the repressor in the absence of the inductor sugar at increasing pressures from atmospheric pressure to 1200 bar (A) and in 2 mM FBP solutions from atmospheric pressure to 1700 bar (B). (C) Average emission wavelength as a function of pressure calculated as described in Materials and Methods in the absence (triangles) and in the presence (squares) of 2 mM FBP. The concentration of protein was 25 μM. All spectra were recorded upon excitation at 295 nm.

used to monitor the effects of high pressure on the repressor structure both in the presence and in the absence of the inducer sugar.

At atmospheric pressure, the fluorescence emission spectrum recorded for native CggR was rather blue-shifted, typical of tryptophan emission for residues buried inside a globular protein (Figure 6A and B). This is in accordance with the recently determined X-ray structure of the regulatory domain of *B. subtilis* CggR (PDB#20KG) which showed the unique Trp residue at the dimer interface. The high intensities measured at short wavelengths (due to scattering of the excitation light, particularly enhanced in the high-pressure cell) indicated the presence of higher order oligomers in the solution. No detectable shift of the fluorescence emission maximum was observed upon addition of 10 mM FBP, even at CggR concentrations as low as 1.2 μM (data not shown). This indicated that the Trp residues of dimeric CggR remain buried upon inducer binding and, hence, that FBP does not lead to dissociation of CggR dimer into monomers under native conditions at micromolar concentrations.

Application of increasing pressure to 25 μM CggR samples in the absence and in the presence of 2 mM FBP resulted in a red shift of the fluorescence peak to around 355 nm (Figure

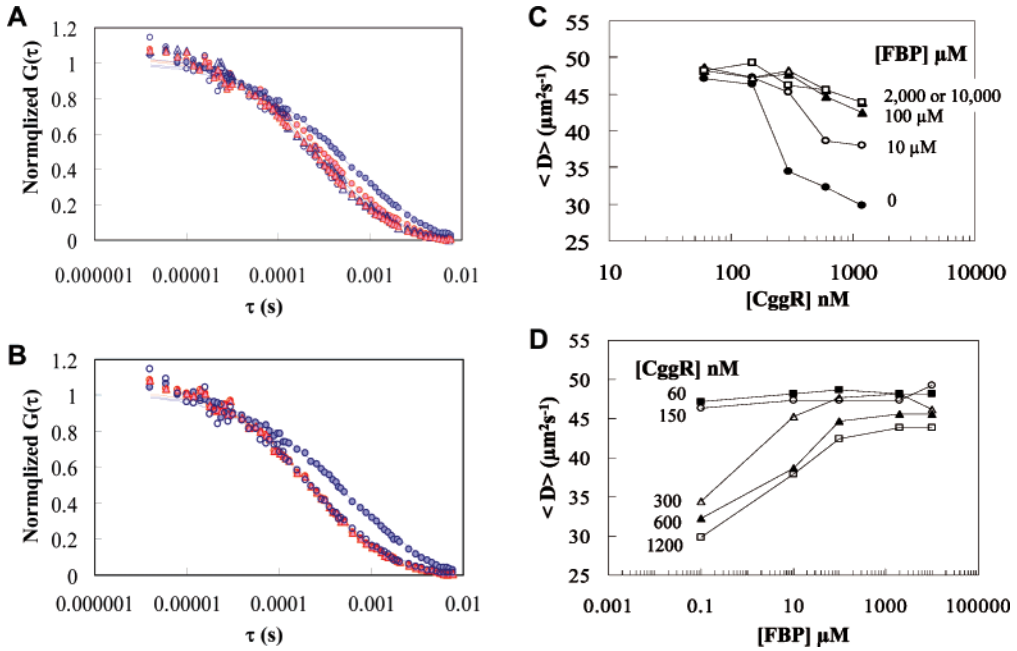

FIGURE 7: Fluorescence correlation profiles of CggR as a function of FBP concentration determined using TMR labeled CggR and two-measurements. (A) Normalized autocorrelation curves recorded at 1.2 μM CggR in the absence (closed blue circles) and in the presence of 10 μM (red circles), 100 μM (blue triangles), 2 mM (red triangles) and 10 mM (open blue circles) FBP. (B) Normalized autocorrelation curves registered at 1.2 μM CggR in the absence (closed blue circles) and in the presence (open red circles) of 10 mM FBP and at 60 nM CggR in the absence (open blue circles) and in the presence (full red triangles) of 10 mM FBP. The fitting functions shown in the graphs correspond to best fitting of the experimental data to a two independent diffusing species model. (C) $\langle D \rangle$ as a function of repressor concentration in the absence (closed circle) and in the presence of 10 μM (open circles), 100 μM (closed triangles), 2 mM (open triangles) and 10 mM (closed squares) FBP. (D) $\langle D \rangle$ as a function of FBP concentration at 1.2 μM (open squares), 600 nM (closed triangles), 300 nM (open triangles), 150 nM (open circles) and 60 nM (closed squares) CggR. The errors in the data are not shown for the shake of clarity.

6A and B), consistent with full exposure of the tryptophan residues to the aqueous solution. In the absence of FBP the transition occurred between 400 and 700 bar, whereas in the presence of 2 mM inducer this transition was shifted to significantly higher pressure, ~1 kbar, providing clear evidence for an FBP dependent stabilization of the repressor against pressure perturbation (Figure 6C). We did not fit these data quantitatively to a dissociation transition because, at 26 μM protein, we know from the AUC experiments that we have a mixture of oligomeric species of undetermined stoichiometry. Thus we do not have an appropriate model to use for determining the stability extrapolated to atmospheric pressure, nor the volume changes of the transitions. It is interesting to note, nonetheless, that the transition in the presence of FBP is much less steep than that in its absence, indicative of a smaller overall apparent volume change, perhaps due to the fact that the oligomeric species are on average smaller in the presence of inducer. Control experiments performed in the presence of 2 mM fructose instead of FBP showed no difference with respect to the profiles determined in the absence of sugar (results not shown), demonstrating that the observed effect arises from specific binding of the inducer sugar to the repressor. Thus, in addition to diminishing the size of CggR higher order oligomers, FBP binding also stabilizes CggR dimers against dissociation into monomers upon the application of pressure. According to the crystal structure, the tryptophan would be exposed to solvent in the folded monomeric repressor. Hence, we cannot conclude whether the high-pressure CggR monomer is folded or unfolded.

FBP Limits Self-Association of CggR Molecules. The above-described experimental data have clearly demonstrated that CggR dimers tend to self-associate to form reversible, high order oligomers in solution, and that FBP disfavors this association. However, except for the fluorescence anisotropy titration, these experiments (due to detection limitations of the techniques) were carried out using micromolar concentrations of CggR, relatively far removed from the more physiologically relevant nanomolar concentration range. Indeed the reported concentration of CggR in *Bacillus subtilis* cells is around 15 nM (*28*) and the binding constant of the repressor to its operator DNA sequence is in the nanomolar range as well (*4*, *12*). In order to investigate the quaternary structure of CggR and the effect of FBP binding at low protein concentration, we turned to the much more sensitive fluorescence correlation spectroscopy (FCS) technique.

Autocorrelation curves were acquired on samples of TMR-labeled CggR between 60 nM and 1.2 μM in the absence and in the presence of varying concentrations of FBP. The autocorrelation curves obtained at different concentrations of protein and inducer sugar exhibited a shift to faster overall diffusion time scales with either increasing FBP concentration (Figure 7A), decreasing CggR concentration (Figure 7B) or increasing KCl concentrations (data not shown). The curves were best fit by a model involving two independent diffusing components. The translational diffusion coefficients (D) recovered from the fits varied from 50 to 56 $\mu m^2\ s^{-1}$ for the fastest diffusing species, whereas that corresponding to the more slowly diffusing oligomers was always below 10 $\mu m^2\ s^{-1}$ (Table 2). There was a percentage of slow diffusing species (around 10−15%) that remained in the solution, even at low concentrations of the protein, under all conditions tested, suggesting that these species may correspond to large irreversible aggregates, which are prob-

Table 2: Translational Diffusion Parameters of CggR as a Function of FBP Concentration[a]

	[CggR] = 1200 nM		[CggR] = 600 nM		[CggR] = 300 nM		[CggR] = 150 nM		[CggR] = 60 nM	
[FBP] (mM)	f_{fast} (%)	$\langle D \rangle$ ($\mu m^2/s$)	f_{fast} (%)	$\langle D \rangle$ ($\mu m^2/s$)	f_{fast} (%)	$\langle D \rangle$ ($\mu m^2/s$)	f_{fast} (%)	$\langle D \rangle$ ($\mu m^2/s$)	f_{fast} (%)	$\langle D \rangle$ ($\mu m^2/s$)
0	53 ± 2	30	57 ± 2	32	56 ± 3	34	82 ± 3	46	84 ± 2	47
0.01	71 ± 2	38	71 ± 2	39	78 ± 2	45	84 ± 3	47	86 ± 2	48
0.1	81 ± 2	42	84 ± 2	45	83 ± 4	48	84 ± 4	47	87 ± 2	49
2	84 ± 2	44	86 ± 2	46	84 ± 1	48	84 ± 1	47	86 ± 2	48
10	84 ± 2	44	86 ± 2	46	80 ± 1	46	88 ± 4	49	86 ± 2	48

[a] Autocorrelation functions were globally fitted to a model involving two translational diffusion coefficients, $D_{fast} = 53 \pm 2\ \mu m^2/s$, and $D_{slow} = 6.3 \pm 0.5\ \mu m^2/s$, which were linked across the profiles recovered at different FBP concentrations for each CggR concentration. In the table, the fractional contribution of the fast diffusing species f_{fast} is shown together with the average translational diffusion coefficient calculated as explained in the main text. Recovered χ^2 was always lower than 1.

ably out of the thermodynamic equilibrium. However, the percentage of fast diffusing species was nonetheless strongly protein concentration dependent. Its fractional abundance increased significantly upon dilution, from 53% at 1.2 μM CggR, to 84% at 60 nM CggR (Table 2). Interestingly, the *D* recovered for this fast diffusing species in the absence of FBP (53 ± 2 $\mu m^2\ s^{-1}$) is compatible with that predicted by the hydrodynamic models we built for dimeric CggR (53−54 $\mu m^2\ s^{-1}$), whereas the CggR monomer would display a theoretical *D* of 64 $\mu m^2\ s^{-1}$. From the fractional contributions and values of the two diffusion components (Table 2) one can calculate an average diffusion coefficient, $\langle D \rangle$. As can be seen in Figure 7C, in the absence of FBP, the average diffusion coefficient decreases significantly with increasing CggR concentration, demonstrating that CggR dimers self-associate in higher order oligomers at concentrations above 150 nM.

The effect of the inducer sugar FBP on the autocorrelation curves recovered for CggR was found to be highly dependent on both CggR and FBP concentration. Thus, at low CggR concentrations, addition of FBP up to 10 mM had no detectable effect on CggR diffusion (Figure 7A−D). In contrast, addition of FBP to more concentrated CggR solutions resulted in a considerable increase in the average diffusion coefficient. At 1.2 μM CggR, the fraction of fast diffusing CggR species increased from 53% in the absence of FBP to 84% in the presence of 10 mM concentration of the inducer sugar (Table 2), and the average diffusion coefficient increased to the values observed at 60 nM CggR (Figure 7D). It should be noted that the effect of FBP binding on the translational diffusion of CggR is observed over four log units of sugar concentration (Figure 7D), indicating that FBP binding, both to the high affinity site and to the low affinity inducer site, disfavors CggR self-association. FCS experiments performed at different ionic strengths (data not shown) demonstrated that addition of KCl concentrations above 200 mM to 1.2 μM CggR solutions results in a progressive increase in the $\langle D \rangle$, consistent with oligomer dissociation. This result indicates that the association of CggR into higher order oligomers involves a significant electrostatic contribution.

FBP Favors CggR Dimers. To further investigate the self-association properties of CggR we carried out cross-correlation experiments on solutions containing a mixture of alexa 488 and atto 647N labeled CggR, up to a total 700 nM repressor concentration, in the absence and in the presence of 10 mM FBP. FCS cross-correlation is a powerful tool for the detection and analysis of species in which two

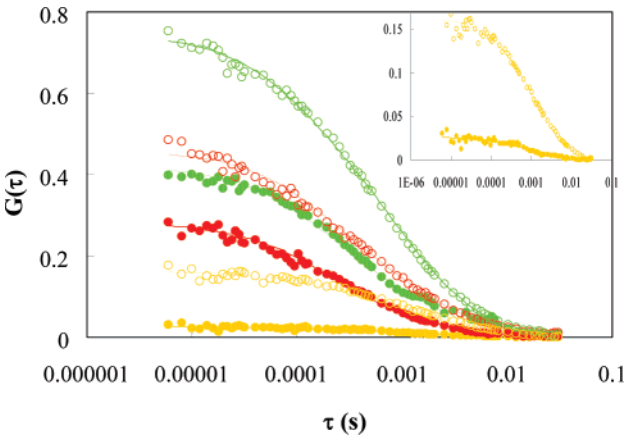

FIGURE 8: Autocorrelation and cross-correlation curves recovered for a mixture of alexa 488-CggR and atto 647N-CggR in the presence (full circles) and in the absence (open circles) of 10 mM FBP. Autocorrelation curves corresponding to the molecules bearing the alexa 488 fluorophore are in green, and those corresponding to the molecules labeled with atto 647N are in red. The cross-correlation function, which arises from the species bearing the two dyes, is in yellow. These curves are also plotted in the inset. The fits shown correspond to global analysis of all the autocorrelation and cross-correlation curves to the two diffusing species model. The total concentration of CggR was 700 nM.

spectrally different fluorophores diffuse together in the confocal detection volume (*29*, *30*). In our experiments, the two fluorophores, atto 647N and alexa 488, were simultaneously excited by means of a two-photon laser beam at 780 nm to obtain two autocorrelation curves, one for each of the fluorophores, and a cross-correlation curve generated only by the oligomeric species bearing the two dyes. We note that likely due to the tendency to self-associate, the efficiency of labeling was only 10% for the alexa 488 labeled samples and ~50% for the atto 647N labeled samples. Thus, the maximum expected amplitude of the cross-correlation signal was quite low. Nonetheless, our experiments show significant cross-correlation (Figure 8, inset) in the absence as well as in the presence of the inducer sugar. As a control, 6 M guanidine-HCl was added to the samples, which resulted in complete disappearance of the cross-correlation, thus eliminating the possibility of any contribution of channel cross-talk to the observed cross-correlation function. Global analysis of the autocorrelation and cross-correlation curves recovered in FBP and in non-FBP containing solutions was performed using a two component model, linking the two diffusion times across all the curves (Table 3). According to the analysis, a 21% fractional contribution of the fast translational diffusion coefficient (~50 $\mu m^2/s$) to the cross-

Table 3: FCS Cross-Correlation Parameters of CggR in the Presence and in the Absence of FBP[a]

	green channel		red channel		cross-correlation	
[FBP] (mM)	f_{fast} (%)	$\langle D \rangle$ ($\mu m^2/s$)	f_{fast} (%)	$\langle D \rangle$ ($\mu m^2/s$)	f_{fast} (%)	$\langle D \rangle$ ($\mu m^2/s$)
0	36 ± 5	22	56 ± 3	31	21 ± 1	15
10	62 ± 9	33	65 ± 3	35	37 ± 5	22

[a] The total concentration of CggR was 700 nM. The curves were fitted in terms of two species with translational diffusion coefficients of 50 ± 2 and 6 ± 1 $\mu m^2/s$. Recovered χ^2 was 0.5. Green, red and cross-correlation channels parameters correspond to CggR species labeled with alexa 488, atto 647N and simultaneously with the two fluorophores, respectively.

correlation function was found in the absence of the inducer sugar which increased to 37% upon addition of 10 mM FBP. These percentages are lower than those recovered from the corresponding autocorrelation curves, which is not surprising since the probability of detecting cross-correlation arising from a dimer is much reduced compared to that arising from a large species involving several CggR units, particularly at low labeling ratios. Nevertheless, the clear contribution of the fast diffusing species to the cross-correlation curve in the absence of FBP indicates that this species is indeed a dimer, not a monomer. Even more interestingly, the contribution of the fast diffusing species to the cross-correlation curves does not diminish upon FBP binding, as would be expected if inducer promoted dimer dissociation, but it was further enhanced, leading to the conclusion that FBP increases the proportion of dimers in CggR solutions.

DISCUSSION

In this work we sought to assess the specific role of FBP binding to the repressor protein CggR, in order to gain a better understanding of the unique mechanism of *gapA* transcription induction by FBP recently proposed (*12*). We demonstrated previously that the effect of FBP on operator binding by CggR required inducer sugar concentrations above 100 μM. In this prior study we detected, as well, a change in the structural dynamics of the CggR/operator complexes at concentrations of inducer between 1 and 100 μM, and suggested based on these results the existence of a second FBP binding site of significantly higher affinity than that involved in induction. Here we show by anisotropy-based FBP titrations of TMR labeled CggR, ITC experiments and limited proteolysis that, in addition to the low affinity binding site responsible for induction, a high affinity site with a K_d of around 6 μM does indeed exist. The structural and dynamic studies reported here suggest strongly that this high affinity site corresponds to the substrate binding site conserved from the homologous enzymes and that it plays a structural role in CggR.

Interestingly, in the recently determined crystal structure of the *B. subtilis* CggR regulatory domain, we noticed important differences in the 3D structure of the two polypeptide chains forming the crystallized dimeric unit. In this structure, one of the polypeptide chains is seen in complex with a molecule of glyceraldehyde-3-phosphate (G3P) while the other is free of sugar ligand (Figure 9). Structural differences are mainly observed for residues forming the proposed high affinity binding site for FBP, in particular Arg250/Arg251, as well as in a surface loop which appears partly disordered in the sugar-free form (see the legend of Figure 9 for more details). From these observations, we hypothesize that binding of a sugar phosphate at the high affinity site assists the complete folding of the CggR molecules which otherwise tend to self-associate and form higher order oligomers. Moreover, our homology modeling and site-directed mutagenesis analysis of the CggR structure predicts, in addition to the sugar substrate binding site, the existence of a second sugar phosphate binding site involving a surface loop, on the basis of the repressor homology with

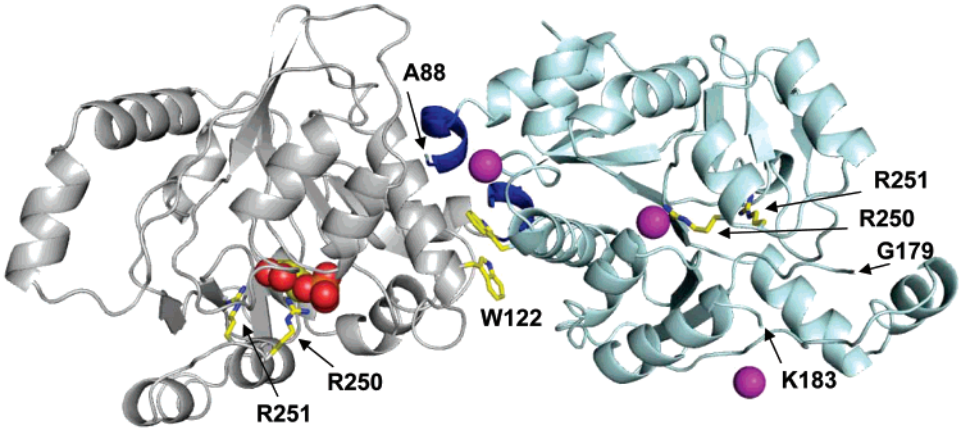

FIGURE 9: Ribbon drawing of the dimeric C-terminal domain of *B. subtilis* CggR (residue 88−338) as seen in the crystal structure deposited in the Protein Data Bank (PDB 2OKG) by P. Rezacova, S. F. Moy, A. Joachimiak and Z. Otwinowski from the Midewest Center for Structural Genomics. For each monomer, the first visible helix linking the N-terminal DNA-binding domain (not seen in this crystal structure) to the regulatory domain is shown in dark blue and the unique tryptophan side-chain (W122) of CggR is shown as yellow sticks. As predicted from modeling studies (*37*), this domain is homologous to glucosamine-6-phosphate deaminases from the NagB family and is capable of binding phosphorylated sugar compounds. In the subunit colored in gray, one molecule of glyceraldehyde-3-phosphate (G3P, shown as red (O atoms), yellow (C atoms) and orange (P atoms) spheres) is bound at the conserved substrate binding site proposed to constitute the high affinity site for FBP in CggR. Also highlighted are the side-chains of Arg250 and Arg251 where trypsin cleavage occurs in the absence of FBP. In the sugar-free polypeptide chain (colored in cyan), these Arg side-chains adopt a different conformation, the internal substrate cavity is more open and part of a surface loop (residues 179−183) is disordered. Three chloride ions (magenta balls) have also been assigned in the crystal structure: one substitutes for the phosphate atom of G3P in the sugar-free monomer, while the others are located at protein−protein interfaces in the crystal lattice. One of these later may indicate the position of the secondary, low affinity site for FBP responsible of the induction mechanism.

allosterically regulated glucosamine-6P-deaminases from the NagB family (see below). It is this second, allosteric site that we propose to be responsible for induction. We show here that FBP binding at this allosteric site, as well as at the high affinity site, interferes with protein−protein interactions and leads to the dissociation of CggR oligomers while favoring CggR dimers.

All together, our results suggest that the effect of FBP on CggR is bimodal. FBP bound to the internal high affinity site ($K_d \sim 6$ μM) acts as a structural cofactor for CggR. Under physiological concentrations of FBP regardless of growth conditions, this site should be constitutively saturated. The role of the second, low affinity site ($K_d > 100$ μM) is to remain responsive to changes in growth conditions, thereby allowing induction through a decrease in CggR operator binding cooperativity. The low affinity of the regulation site for the inducing sugar is consistent with the fact that intracellular FBP concentration increases to 7−14 mM under glycolytic conditions. In the case of CggR, changes in the cooperative DNA binding mode might be explained by FBP-driven alternative dimer−dimer interactions upon binding to the low affinity site, thus modifying the structure and stability of the tetrameric repressor and hence the cooperativity of DNA binding. Other mechanisms of enzyme modulation by FBP have also been shown to be linked to the quaternary structure of the target enzyme, through selective stabilization of active or inactive oligomeric forms (*31*). Furthermore, in micro-organisms, FBP frequently plays the role of an allosteric effector of enzymes involved in sugar metabolism (*32*, *33*). It is therefore not surprising that conformational changes are observed in CggR upon inducer binding. Finally, the stabilization effect we report here for CggR has already been observed for other proteins in which FBP binding leads to stabilization through loop ordering (*34*).

Evolutionarily, the regulatory domain of CggR is not structurally related to any protein that binds FBP as a substrate or effector molecule, but seems to have evolved from enzymes of the NagB family which use 6-phosphohexoses or -hexosamines as substrates, products or allosteric activators (*37*). In the hexameric allosteric glucosamine-6-phosphate deaminase from *Escherichia coli* (*Eco*NagB), the transition from the inactive T-conformer to the activated R-state is associated with tertiary and quaternary structure rearrangements driven by conformational changes within a flexible loop region. This region comprises a so-called active-site lid that folds over the catalytic center and contains residues forming both the internal cavity for the substrate (glucosamine-6-phosphate) and the inter-subunit contact surface where the activator (*N*-acetylglucosamine-6-phosphate) binds. This lid is highly disordered in the ligand-free T-conformer, while it adopts a conformation able to bind effectors at the allosteric site in the R-conformation, thereby modifying inter-subunit contacts and the cooperative catalytic efficiency of the enzyme subunits (*35*, *36*). This regulation mechanism is strikingly similar to the one we propose for CggR, although in case of this repressor, the same effector molecule (FBP) binds at both the substrate and allosteric sites, but with different affinity. The evolutionary challenge for regulation of the *gap* operon by FBP resides in the necessity for a low affinity, yet highly specific binding site for FBP. Unlike the lactose repressor that retained the high affinity sugar binding site as its inducer binding site, CggR has retained the high affinity sugar binding site, but due to the high physiological concentrations of FBP, not for inducer function. Rather, the sugar substrate site has been maintained as a structural cofactor site, and an additional low affinity site, perhaps evolved from the enzymatic allosteric sites, serves to modulate gene expression.

ACKNOWLEDGMENT

The authors thank Dr. Stefan Arold for his help with the ITC experiments.

REFERENCES

1. Fillinger, S., Boschi-Muller, S., Azza, S., Dervyn, E., Branlant, G., and Aymerich, S. (2000) Two glyceraldehyde-3-phosphate dehydrogenases with opposite physiological roles in a nonphotosynthetic bacterium, *J. Biol. Chem. 275*, 14031−14037.
2. Ludwig, H., Rebhan, N., Blencke, H. M., Merzbacher, M., and Stulke, J. (2002) Control of the glycolytic gapA operon by the catabolite control protein A in Bacillus subtilis: a novel mechanism of CcpA-mediated regulation, *Mol. Microbiol. 45*, 543−553.
3. Kunst, F., Ogasawara, N., Moszer, I., Albertini, A. M., Alloni, G., Azevedo, V., Bertero, M. G., Bessieres, P., Bolotin, A., Borchert, S., Borriss, R., Boursier, L., Brans, A., Braun, M., Brignell, S. C., Bron, S., Brouillet, S., Bruschi, C. V., Caldwell, B., Capuano, V., Carter, N. M., Choi, S. K., Codani, J. J., Connerton, I. F., and Danchin, A. (1997) The complete genome sequence of the gram-positive bacterium Bacillus subtilis, *Nature 390*, 249−256.
4. Doan, T., and Aymerich, S. (2003) Regulation of the central glycolytic genes in Bacillus subtilis: binding of the repressor CggR to its single DNA target sequence is modulated by fructose-1,6-bisphosphate, *Mol. Microbiol. 47*, 1709−1721.
5. Saxild, H. H., Andersen, L. N., and Hammer, K. (1996) Dra-nupC-pdp operon of Bacillus subtilis: nucleotide sequence, induction by deoxyribonucleosides, and transcriptional regulation by the deoR-encoded DeoR repressor protein, *J. Bacteriol. 178*, 424−434.
6. Zeng, X., Saxild, H. H., and Switzer, R. L. (2000) Purification and characterization of the DeoR repressor of Bacillus subtilis, *J. Bacteriol. 182*, 1916−1922.
7. Stulke, J., and Hillen, W. (2000) Regulation of carbon catabolism in Bacillus species, *Annu. Rev. Microbiol. 54*, 849−880.
8. Yoshida, K., Fujimura, M., Yanai, N., and Fujita, Y. (1995) Cloning and sequencing of a 23-kb region of the Bacillus subtilis genome between the iol and hut operons, *DNA Res. 2*, 295−301.
9. Dombrauckas, J. D., Santarsiero, B. D., and Mesecar, A. D. (2005) Structural basis for tumor pyruvate kinase M2 allosteric regulation and catalysis, *Biochemistry 44*, 9417−9429.
10. Yu, P., and Pettigrew, D. W. (2003) Linkage between fructose 1,6-bisphosphate binding and the dimer-tetramer equilibrium of Escherichia coli glycerol kinase: critical behavior arising from change of ligand stoichiometry, *Biochemistry 42*, 4243−4252.
11. Cameron, A. D., Roper, D. I., Moreton, K. M., Muirhead, H., Holbrook, J. J., and Wigley, D. B. (1994) Allosteric activation in Bacillus stearothermophilus lactate dehydrogenase investigated by an X-ray crystallographic analysis of a mutant designed to prevent tetramerization of the enzyme, *J. Mol. Biol. 238*, 615−625.
12. Zorrilla, S., Doan, T., Alfonso, C., Margeat, E., Ortega, A., Rivas, G., Aymerich, S., Royer, C. A., and Declerck, N. (2007) Inducer-modulated cooperative binding of the tetrameric CggR repressor to operator DNA, *Biophys. J. 92*, 3215−3227.
13. Schuck, P., Perugini, M. A., Gonzales, N. R., Howlett, G. J., and Schubert, D. (2002) Size-distribution analysis of proteins by analytical ultracentrifugation: strategies and application to model systems, *Biophys. J. 82*, 1096−1111.
14. Laue, T. M., Shaw, B. D., Ridgeway, T. M., and Pelletier, S. L. (1992) Computer-aided interpretation of analytical sedimentation data for proteins, in *Analytical Ultracentrifugation in Biochemistry and Polymer Science* (Harding, S. E., Rowe, A. J., Horton, J. C., Eds.) pp 90−125, The Royal Society of Chemistry, Cambridge, U.K.
15. Garcia de la Torre, J., Huertas, M. L., and Carrasco, B. (2000) Calculation of hydrodynamic properties of globular proteins from their atomic-level structure, *Biophys. J. 78*, 719−730.

16. Fernandes, M. X., Bernado, P., Pons, M., and Garcia de la Torre, J. (2001) An analytical solution to the problem of the orientation of rigid particles by planar obstacles. Application to membrane systems and to the calculation of dipolar couplings in protein NMR spectroscopy, *J. Am. Chem. Soc. 123*, 12037−12047.
17. Garcia de la Torre, J., and Carrasco, B. (2002) Hydrodynamic properties of rigid macromolecules composed of ellipsoidal and cylindrical subunits, *Biopolymers 63*, 163−167.
18. Royer, C. A., Smith, W. R., and Beechem, J. M. (1990) Analysis of binding in macromolecular complexes: a generalized numerical approach, *Anal. Biochem. 191*, 287−294.
19. Royer, C. A., and Beechem, J. M. (1992) Numerical analysis of binding data: advantages, practical aspects, and implications, *Methods Enzymol. 210*, 481−505.
20. Royer, C. A. (1993) Improvements in the numerical analysis of thermodynamic data from biomolecular complexes, *Anal. Biochem. 210*, 91−97.
21. Berland, K., and Shen, G. (2003) Excitation saturation in two-photon fluorescence correlation spectroscopy, *Appl. Opt. 42*, 5566−5576.
22. Vidugiris, G. J., Markley, J. L., and Royer, C. A. (1995) Evidence for a molten globule-like transition state in protein folding from determination of activation volumes, *Biochemistry 34*, 4909−4912.
23. Garcia de la Torre, J. (1994) Hydrodynamics of segementally flexible macromolecules, *Eur. Biophys. J. 23*, 307−322.
24. Silva, J. L., and Weber, G. (1993) Pressure stability of proteins, *Annu. Rev. Phys. Chem. 44*, 89−113.
25. Royer, C. A. (2002) Revisiting volume changes in pressure-induced protein unfolding, *Biochim. Biophys. Acta 1595*, 201−209.
26. Weber, G., and Drickamer, H. G. (1983) The effect of high pressure upon proteins and other biomolecules, *Q. Rev. Biophys. 16*, 89−112.
27. Zipp, A., and Kauzmann, W. (1973) Pressure denaturation of metmyoglobin, *Biochemistry 12*, 4217−4228.
28. Meinken, C., Blencke, H. M., Ludwig, H., and Stulke, J. (2003) Expression of the glycolytic gapA operon in Bacillus subtilis: differential syntheses of proteins encoded by the operon, *Microbiology 149*, 751−761.
29. Medina, M. A., and Schwille, P. (2002) Fluorescence correlation spectroscopy for the detection and study of single molecules in biology, *Bioessays 24*, 758−764.
30. Rosales, T., Georget, V., Malide, D., Smirnov, A., Xu, J., Combs, C., Knutson, J. R., Nicolas, J. C., and Royer, C. A. (2007) Quantitative detection of the ligand-dependent interaction between the androgen receptor and the co-activator, Tif2, in live cells using two color, two photon fluorescence cross-correlation spectroscopy, *Eur. Biophys. J. 36*, 153−161.
31. Shirakihara, Y., and Evans, P. R. (1988) Crystal structure of the complex of phosphofructokinase from Escherichia coli with its reaction products, *J. Mol. Biol. 204*, 973−994.
32. Murcott, T. H., Gutfreund, H., and Muirhead, H. (1992) The cooperative binding of fructose-1,6-bisphosphate to yeast pyruvate kinase, *EMBO J. 11*, 3811−3814.
33. Ormo, M., Bystrom, C. E., and Remington, S. J. (1998) Crystal structure of a complex of Escherichia coli glycerol kinase and an allosteric effector fructose 1,6-bisphosphate, *Biochemistry 37*, 16565−16572.
34. Jurica, M. S., Mesecar, A., Heath, P. J., Shi, W., Nowak, T., and Stoddard, B. L. (1998) The allosteric regulation of pyruvate kinase by fructose-1,6-bisphosphate, *Structure 6*, 195−210.
35. Bustos-Jaimes, I., Sosa-Peinado, A., Rudino-Pinera, E., Horjales, E., and Calcagno, M. L. (2002) On the role of the conformational flexibility of the active-site lid on the allosteric kinetics of glucosamine-6-phosphate deaminase, *J. Mol. Biol. 319*, 183−189.
36. Horjales, E., Altamirano, M. M., Calcagno, M. L., Garratt, R. C., and Oliva, G. (1999) The allosteric transition of glucosamine-6-phosphate deaminase: the structure of the T state at 2.3 Å resolution, *Structure 7*, 527−537.
37. Doan, T., Martin, L., Zorrilla, S., Chaix, D., Aymerich, S., Labesse, G., and Declerck, N. (2007) Phospho-sugar binding (PSB) domain homologous to NagB enzymes regulates the activity of the central glycolytic genes repressor (CggR), *Proteins*, in press.

BI701805E